actuators

MDPI

Article

Autonomous Tracked Vehicle Trajectory Tracking Control Based on Disturbance Observation and Sliding Mode Control

Xihao Yan, Shuo Wang, Yuxin He, Aixiang Ma and Sihai Zhao *

School of Mechanical and Electrical Engineering, China University of Mining & Technology, Beijing 100083, China; bqt2100401009@student.cumtb.edu.cn (X.Y.); bqt2300401003t@student.cumtb.edu.cn (S.W.); bqt2400401003t@student.cumtb.edu.cn (Y.H.); bqt2200401006@student.cumtb.edu.cn (A.M.)
* Correspondence: zsh@cumtb.edu.cn

Abstract: This paper examines the path-tracking control issue for tracked mobile robots (TMRs) operating in complex terrains, focusing on improving their autonomous operation capabilities. Considering the system's complex dynamic model, environmental uncertainties, and non-linear characteristics, especially the phenomenon of track slippage, a dynamic model that incorporates track slippage is proposed. A sliding factor observer is then designed to estimate slippage parameters, ensuring the control system remains stable and accurate despite uncertainties. A hierarchical control architecture is introduced, with the upper-level controller using a kinematic model to generate desired rotational speed commands for the left and right drive wheels. The lower-level controller, operating on a dynamic model, adjusts motor torque to achieve these desired speeds. Utilizing sliding mode control strategies, combined with adaptive laws and nonlinear control methods, the controller effectively addresses the issue of high-frequency chattering arising from the use of signum functions, thereby enhancing the lifespan of actuators and overall system control performance. A comprehensive simulation and experimental setup for real TMR systems is established to validate the proposed control strategy. Results demonstrate that the control scheme effectively achieves trajectory tracking across various unstructured terrains, exhibiting strong robustness and stability.

Keywords: tracked mobile robot; trajectory tracking control; disturbance observer; sliding mode control

Academic Editors: Md Abdus Samad Kamal and Masakazu Mukai

Received: 9 January 2025
Revised: 19 January 2025
Accepted: 21 January 2025
Published: 24 January 2025

Citation: Yan, X.; Wang, S.; He, Y.; Ma, A.; Zhao, S. Autonomous Tracked Vehicle Trajectory Tracking Control Based on Disturbance Observation and Sliding Mode Control. *Actuators* **2025**, *14*, 51. https://doi.org/10.3390/act14020051

1. Introduction

Compared to traditional wheeled robots, tracked robots exhibit superior traversing capability and terrain adaptability, which makes them widely utilized in operational scenarios with unstructured surfaces in military, agricultural, and industrial applications [1]. With continuous advancements in autonomous driving technology and the growing demand for automation in special mission conditions, the technology of unmanned tracked vehicles has experienced rapid development in recent years [2]. Path tracking technology, as a crucial component of autonomous operation for tracked vehicles, has garnered significant attention from both industry and academia [3].

Despite the evident advantages of tracked vehicles in complex environments, their path tracking control remains a challenging issue. The primary reasons include the complexity of the dynamic model of tracked vehicles, the extensive distribution of environmental variables, the highly nonlinear nature of the system, and the presence of non-holonomic constraints [4]. Specifically, tracked vehicles rely on differential steering, a mechanism that depends on the slip generated by the tracks, necessitating the incorporation of unknown

friction and other external disturbances into the vehicle's dynamic model, which are difficult to accurately describe with conventional modeling techniques [5]. In unpaved driving environments, due to the complexity of ground adhesion conditions, parameter creep, and external disturbances, control performance can easily deteriorate [6]. To address the model uncertainty issues of tracked mobile robots (TMRs), a high-speed tracked vehicle dynamics simulation method based on model reduction strategies was proposed in [7]. In [8], a simplified track multibody dynamics model was derived and integrated by deducing the dynamic model of a dual differential steering transmission and the multibody model of tracked vehicles. In [9], a longitudinal-vertical coupled dynamics model for tracked vehicles operating on rough terrain was established, revealing the significant influence of vehicle speed and road roughness on the longitudinal dynamics of the vehicle. In conclusion, the kinematic model alone is insufficient to fully describe the behavior of TMRs; the effects of dynamics must also be taken into account.

To address these challenges, state and disturbance observation methods have also been widely applied in TMRs. In [10], a steering controller for tracked vehicles that combines parameter adaptive laws and a second-order disturbance observer (DO-2) was proposed, capable of online estimation of friction coefficients and resistance against random disturbances. In [11], a traditional sensor-based algorithm for estimating driving parameters was introduced, which can estimate the longitudinal force and vehicle speed. In [12], a kinematic model integrated with slip parameter estimation was proposed, utilizing extended Kalman filtering (EKF) and improved sliding mode observer (ISMO) methods to estimate slip parameters. These studies indicate that observing external disturbances and system states can effectively enhance the performance of controllers.

Based on the aforementioned model establishment and state observation schemes, the control problems of TMRs primarily focus on a variety of control strategies, including PID control, backstepping control, and model predictive control. In [13], a hybrid control architecture combining MIMO data-driven control and sliding mode control was proposed for addressing the path tracking problem of autonomous unmanned ground vehicles in precision agriculture on rough terrain. In [14], an integrated method based on Hybrid A* path planning and adaptive model predictive control (AMPC) was proposed to solve the trajectory planning and tracking control issues for articulated tracked vehicles. In [15], a comprehensive modeling method and trajectory tracking control strategy for autonomous tracked vehicles, integrating a backstepping controller and integral sliding mode control of vehicle drive torque, were proposed. In [16], a control scheme based on a third-order fixed-time extended state observer and a zeroing neural network was presented, which estimates unknown lumped disturbances and unmeasurable speeds, achieving convergence of observation errors to zero within a fixed time.

Sliding Mode Control (SMC) has demonstrated significant advantages in trajectory control of tracked vehicles, primarily due to its robustness and insensitivity to parameter variations and external disturbances. Compared to traditional PID controllers, SMC is better suited to handle nonlinear systems and uncertainties, ensuring stability and precise tracking performance for tracked vehicles in complex terrains and dynamic environments. Additionally, SMC offers lower computational requirements compared to other robust controllers, and its design is relatively straightforward, not requiring an accurate system model. This makes SMC more flexible and reliable in practical applications [17]. However, sliding mode control can easily lead to high-frequency chattering due to the sign function, which may exacerbate actuator wear and degrade system performance [18]. To solve the chattering problem, a continuous super-twisting control (STC) method based on high-order sliding mode observers (HOSMO) was proposed in [19], successfully achieving second-order sliding mode (SOSM) on the selected sliding surface. In [20], a robust continuous

sliding mode control (CSMC) method combined with a nonlinear disturbance observer (NDO) for disturbance estimation and compensation was proposed, constructing a cascaded control framework. The superiority of the controller in disturbance suppression and robustness against disturbances was verified through simulations and experiments, along with a stability analysis of the system.

In off-road driving environments, the complexity of ground adhesion conditions, parameter uncertainties, creep characteristics, and external disturbances can all lead to significant degradation in the effectiveness of conventional path tracking control. This is especially pronounced when the vehicle operates on challenging terrains such as flooded or muddy surfaces, where the intricate contact conditions between the tracks and the ground, as well as the uncertain relationship between slip ratio and driving force, further amplify the discrepancies between the ideal motion model and actual vehicle response [21]. Reference [22] introduces a slip model based on the instantaneous centers of rotation (ICRs) of the tracks and a dual-adaptive unscented Kalman filter (DAUKF), which significantly improves the accuracy and practicality of intelligent tracked vehicle models in complex terrains by real-time estimation of ICR positions. Reference [23] proposes a path tracking control method that integrates a Sup controller with PID and SMC, modifying the lateral error slightly and optimizing the approach through particle swarm optimization (PSO). Reference [24] analyzes the influence of inertial forces on the position of the instantaneous center of rotation (ICR) of the tracks, proposing a new kinematic model based on dynamic simulations on hard, level ground. This model estimates the actual ICR positions of the tracks using three indices: slip, eccentricity, and steering efficiency. Given the above discussion, SMC, with its robustness and low computational complexity, presents a viable solution for real-time trajectory tracking control of TMRs in the presence of slipping disturbances.

The trajectory tracking accuracy of TMRs is often compromised due to slip caused by differential turning. To address this issue, this paper proposes a super-twisting sliding mode controller based on a disturbance observer. First, a TMR model that considers slip is established, taking into account the system's nonlinearity and track slip. Based on this system model, a slip factor observer is designed, and its stability is analyzed. Subsequently, a hierarchical controller is designed: the upper-level controller, based on the kinematic model, generates the desired rotational speed signals for the left and right drive wheels; the lower-level controller, based on the dynamic model of the tracks, adjusts the motor torque output according to the desired rotational speed signals, collectively achieving the pose control of the TMRs. Finally, a simulation environment and experimental environment are established based on a real TMR system to thoroughly validate the effectiveness of the controller. The contributions of this study are twofold:

1. The track slip is treated as a lumped external disturbance, and a track slip factor observer is designed, which features only one adjustable parameter, thereby avoiding complex parameter tuning.
2. Unlike most studies on tracked vehicles that only consider kinematic models, this research comprehensively incorporates the dynamic model of the tracks. A hierarchical controller is designed to achieve precise trajectory tracking control.

The structure of this paper is as follows: Section 1 introduces the research background and significance; Section 2 establishes the dynamics model of TMRs; Section 3 designs the slip factor observer and presents the design method of the hierarchical controller; Section 5 validates the effectiveness of the controller through simulations and experiments; and Section 5 summarizes and prospects the entire paper.

2. TMRs Modeling

2.1. TMRs Kinematic Model

Remark 1. *In this paper, the subscript L denotes the local coordinate system of the robot; if there is no subscript, it indicates that the parameter is in the global coordinate system; the subscript l denotes the parameter located on the left track in the direction of travel, and the subscript r denotes the parameter located on the right track in the direction of travel.*

Figure 1 shows the top view of TMR kinematic model. The kinematic model of a track-type mobile robot is given by:

$$q = \begin{pmatrix} \dot{x} \\ \dot{y} \\ \dot{\varphi} \end{pmatrix} = \begin{pmatrix} \cos\varphi & 0 \\ \sin\varphi & 0 \\ 0 & 1 \end{pmatrix} \begin{pmatrix} v \\ \omega \end{pmatrix} \tag{1}$$

where θ is the yaw angle, v is the linear velocity of the robot, and w is the angular velocity. Equation (1) does not explicitly consider the sliding effect between the tracks and the ground. In practice, the most direct cause of sliding is the imbalance between the frictional force and the torque output by the track drive motors. However, due to the complexity of modeling friction, sliding effects are generally not modeled by directly analyzing friction, but rather through kinematic analysis. From a holistic perspective, the motion of a mobile robot can be considered as circular motion around an instantaneous center of rotation O_c. When sliding effects are present, O_c is offset from the O_L axis by a distance ε, which can be expressed as:

$$\begin{aligned} \varepsilon &= \tfrac{Lv^2}{2\mu_t g R'} \sin\alpha \\ \alpha &= \arctan(\tfrac{v_{YL}}{v_{XL}}) \end{aligned} \tag{2}$$

where α is the side slip angle. It is important to note that the offset ε cannot exceed the position of the track drive wheels' axis, denoted as "$|\varepsilon| \leq L/2 - r$". In the presence of sliding, the actual linear velocities of the left and right drive wheels are affected by sliding parameters. The actual linear velocities of the left and right wheels can be expressed as:

$$\begin{aligned} v_l &= r\omega_l(1 - s_l) \\ v_r &= r\omega_r(1 - s_r) \end{aligned} \tag{3}$$

where w_l and w_r are the rotational speeds of the drive wheels, r is the radius of the drive wheels, v_l and v_r are the actual forward speeds of the left and right tracks, and s_l and s_r are the longitudinal slip ratios of the left and right tracks. The side slip turning radius R' can be expressed as:

$$R' = \frac{||v_B||}{|\omega|} = \frac{b}{2\cos\alpha} \frac{\omega_l(1 - s_l) + \omega_r(1 - \sigma_r)}{\omega_l(1 - s_l) - \omega_r(1 - \sigma_r)} \tag{4}$$

where b is the width of the robot. Therefore, v_L can be expressed as:

$$\|v_L\| = \frac{v_l + v_r}{2\cos\alpha} = \frac{r\omega_l(1 - s_l) + r\omega_r(1 - s_r)}{2\cos\alpha} \tag{5}$$

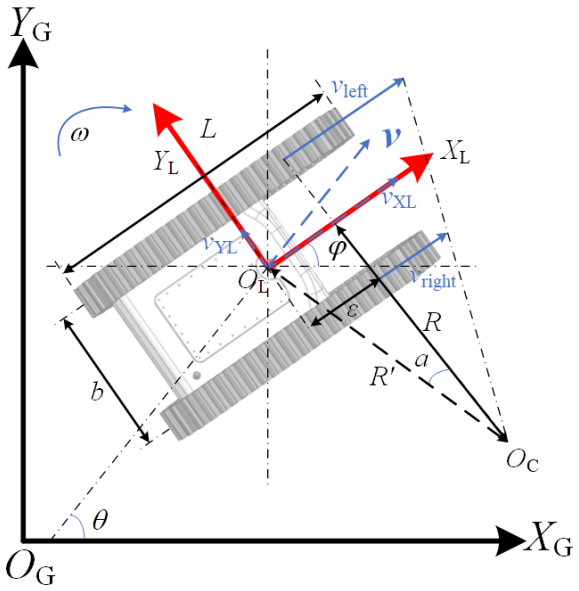

Figure 1. Top View of TMR Kinematic Model.

Converting the vehicle velocity v from the body coordinate system to the global coordinate system, can get:

$$\begin{aligned} v &= \begin{pmatrix} \cos\varphi & -\sin\varphi \\ \sin\varphi & \cos\varphi \end{pmatrix} \begin{pmatrix} \|v_L\|\cos\alpha \\ \|v_L\|\sin\alpha \end{pmatrix} = \|v_L\| \begin{pmatrix} \cos(\varphi+\alpha) \\ \sin(\varphi+\alpha) \end{pmatrix} \\ \dot{\varphi} &= \frac{-r\omega_l(1-s_l)+r\omega_r(1-s_r)}{b} \end{aligned} \tag{6}$$

Substituting (5) into (6) and then into (1), we obtain the kinematic model of a track-type ground mobile robot considering sliding effects:

$$q = \begin{pmatrix} \dot{x} \\ \dot{y} \\ \dot{\varphi} \end{pmatrix} = \begin{pmatrix} \frac{r}{2}(\cos\varphi - \sin\varphi\tan\alpha)((1-s_l)\omega_l + (1-s_r)\omega_r) \\ \frac{r}{2}(\sin\varphi + \cos\varphi\tan\alpha)((1-s_r)\omega_l + (1-s_l)\omega_r) \\ \frac{r}{b}((1-s_l)\omega_l - (1-s_r)\omega_r) \end{pmatrix} \tag{7}$$

where $q = \begin{bmatrix} \dot{x} & \dot{y} & \dot{\varphi} \end{bmatrix}^T$ is the global pose of the mobile robot. Since the track-type vehicle can only move along the normal to the drive sprocket axis, the non-holonomic constraint can be expressed as [25]:

$$-\dot{x}\sin\varphi + \dot{y}\cos\varphi + \dot{\varphi}\varepsilon = 0 \tag{8}$$

The tracking control of a mobile robot with sliding parameters is accomplished in two steps: first, the online estimation of sliding parameters, which can be solved using various nonlinear online estimation methods introduced in Section 3; second, constructing a tracking control law using the estimated sliding parameters to achieve tracking control, which is addressed using nonlinear control methods presented in Section 3.

2.2. TMRs Dynamic Model

As depicted in Figure 2, the forces acting on the tracked vehicle include the traction forces F_l and F_r, the longitudinal resistances R_l and R_r on the left and right tracks, and the transverse frictional force resulting from the distribution of lateral soil shear forces.

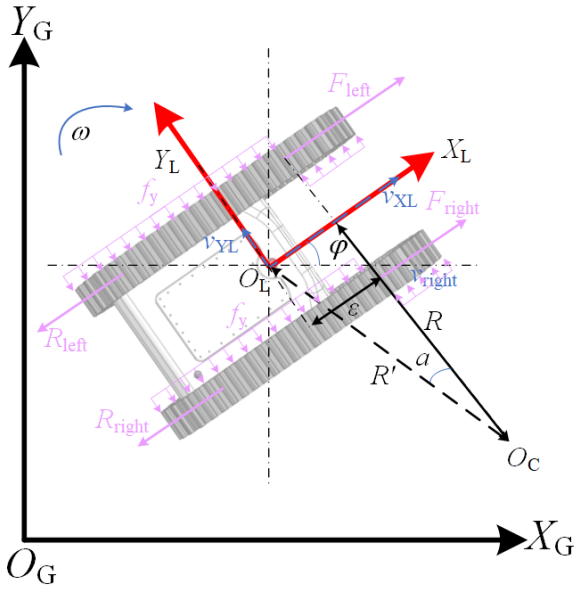

Figure 2. Top View of TMR Dynamic Model.

Assumption 1. *It is assumed that the tracked vehicle has a left–right symmetric physical structure, with the vehicle's weight uniformly distributed across the two tracks. The longitudinal position of the center of mass coincides with the midpoint of the tracks, and the vertical load on the tracks is uniformly distributed. The lateral resistance coefficient μ_t is constant.*

To satisfy the lateral equilibrium condition, the instantaneous center of rotation O_C must be located forward of the Y_L axis at a distance ε. The equations of motion in the vehicle's local reference frame can be expressed as:

$$\begin{aligned} m\ddot{x}_L &= F_r + F_l - R_r - R_l \\ m\ddot{y}_L &= F_y \\ I_z\ddot{\varphi} &= \tfrac{b}{2}(-F_r + F_l) - M_r \end{aligned} \tag{9}$$

where M_r is the steering resistance torque caused by the lateral soil shear distribution force. Specifically:

$$R_l = R_r = \frac{\mu_l mg}{2} \tag{10}$$

Here, μ_l is the rolling resistance coefficient. The lateral force F_y per unit length of track can be expressed as:

$$\begin{aligned} F_y &= 2 \times \textstyle\int_{-L/2}^{L/2} f_y(l_x)dl_x \\ M_r &= 2 \times \textstyle\int_{-L/2}^{L/2} f_y(l_x) \times l_x dl_x \end{aligned} \tag{11}$$

where l_x is the longitudinal distance from the track element to the center of mass, taken positive in the forward direction. Since the lateral force y_f is a sliding frictional force, and under the assumption of uniformly distributed load given earlier, the expressions for the lateral force F_y and the yaw resistance torque M_r are:

$$\begin{aligned} F_y &= \frac{2sgn(\omega)\mu_t \varepsilon mg}{L} \\ M_r &= \frac{(4\varepsilon^2 - L^2)sgn(\omega)\mu_t mg}{4L} \end{aligned} \tag{12}$$

Selecting the track as the object of study, the rotational speed control equation is established. The track is driven by a motor and is subjected to the combined effects of

traction forces and internal and external resistances. The rotational dynamics equation for the track is given by:

$$\begin{aligned} \dot{\omega}_l &= \frac{1}{J}(T_{e,l} - r(F_l + R_l) - \mu_\omega \omega_l) \\ \dot{\omega}_r &= \frac{1}{J}(T_{e,r} - r(F_r + R_r) - \mu_\omega \omega_r) \end{aligned} \tag{13}$$

where J is the total equivalent rotational inertia of the track on one side, T_e is the driving torque of the motor on one side, and μ_ω is the internal rotational resistance of the system.

3. Main Results

3.1. Observer Design

The structure of the control system is illustrated in Figure 3. In practical engineering conditions, the driving force and slip ratio of the tracks are often unmeasurable. Additionally, the variability of ground conditions makes direct driving force control challenging. To achieve accurate path tracking control, it is necessary to start from the kinematic relationship between track rotational speed and vehicle speed, treating lateral slip as part of the disturbance, and design a disturbance observer for slip compensation.

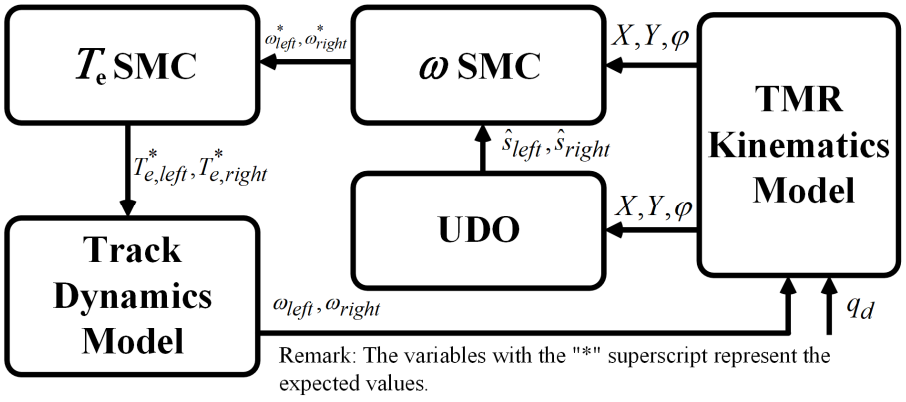

Figure 3. Block Diagram of TMRs Control System.

Define the rotational speeds of the left and right track drive wheels as the system inputs. The vehicle motion model considering track slip can be expressed as:

$$\begin{aligned} v_L &= \overline{v}_L + \widetilde{v}_L = \frac{1}{2}(v_l + v_r) - \frac{1}{2}(v_l s_l + v_r s_r) \\ \omega_L &= \overline{\omega}_L + \widetilde{\omega}_L = \frac{1}{b}(v_l + v_r) - \frac{1}{b}(v_l s_l + v_r s_r) \end{aligned} \tag{14}$$

where the variables with the superscript "-" represent the longitudinal velocities and yaw rates under zero slip conditions, i.e., the ideal kinematic estimates, and the superscript "~" denotes the uncertain quantities caused by track slip. Taking the derivative of both sides of the above equation, we get:

$$\begin{aligned} \dot{v}_L &= \dot{\overline{v}}_L + \dot{\zeta}_v \\ \dot{\omega}_L &= \dot{\overline{\omega}}_L + \dot{\zeta}_\omega \end{aligned} \tag{15}$$

where $\dot{\zeta}_v$ and $\dot{\zeta}_\omega$ are the derivatives of the longitudinal and yaw motion disturbances, respectively, representing the differences between the theoretically calculated velocities and the actual velocities of the tracked vehicle. Combining Equations (7) and (14), the state equations of the kinematic system can be written as:

$$\dot{X}_L = U + \dot{\zeta} \tag{16}$$

where

$$\begin{aligned} \dot{X}_L &= \begin{pmatrix} \dot{v}_{XL} & \dot{v}_{YL} & \dot{\omega}_L \end{pmatrix}^T \\ U &= \begin{pmatrix} \dot{\bar{v}}_{XL} & 0 & \dot{\bar{\omega}}_L \end{pmatrix}^T \\ \dot{\zeta} &= \begin{pmatrix} \dot{\bar{v}}_L & \dot{v}_y & \dot{\bar{\omega}}_L \end{pmatrix}^T \end{aligned} \tag{17}$$

and ζ is the generalized disturbance input for lateral motion. Applying a low-pass filter to the state variables and system inputs [26]:

$$\begin{aligned} \kappa \dot{X}_{Lf} + X_{Lf} &= X_L \\ \kappa \dot{U}_f + U_f &= U \end{aligned} \tag{18}$$

where $\kappa > 0$, and define the auxiliary variable as:

$$\vartheta = \kappa\left(X - X_{Lf}\right) - U_f - \dot{\zeta} \tag{19}$$

Lemma 1. *For system (15) and filtering operation (17), the auxiliary variable ϑ is bounded and exponentially decreases to 0 for $\kappa > 0$. That is, $\vartheta = 0$ is an invariant manifold.*

Proof. Taking the derivative of the auxiliary variable ϑ:

$$\begin{aligned} \dot{\vartheta} &= \kappa\left(\dot{X} - \dot{X}_{Lf}\right) - \dot{U}_f - \ddot{\zeta} \\ &= \kappa(\dot{\zeta} + U_f) - \kappa \dot{X}_{Lf} - \dot{U}_f - \ddot{\zeta} \\ &= -\kappa\left(\kappa(X - X_{Lf}) - BU_f - \dot{\zeta}\right) - \ddot{\zeta} \\ &= -\kappa\vartheta - \ddot{\zeta} \end{aligned} \tag{20}$$

Define the Lyapunov function as:

$$V(\vartheta) = \vartheta^T \vartheta \tag{21}$$

Taking the derivative of $V(\vartheta)$:

$$\begin{aligned} \dot{V} &= 2\vartheta^T \dot{\vartheta} \\ &= 2\vartheta^T(-\kappa\vartheta - \ddot{\zeta}) \\ &= -2\kappa\vartheta^T\vartheta - 2\vartheta^T\ddot{\zeta} \end{aligned} \tag{22}$$

Using Young's inequality, we get:

$$\begin{aligned} \dot{V} &= -2\kappa\vartheta^T\vartheta - 2\vartheta^T\ddot{\zeta} \leq -\epsilon\vartheta^T\vartheta - \tfrac{1}{\epsilon}\dot{\zeta}^T\ddot{\zeta} \\ &\leq -(2\kappa + \epsilon)\vartheta^T\vartheta - \tfrac{1}{\epsilon}\ddot{\zeta}^T\ddot{\zeta} \end{aligned} \tag{23}$$

Since the second derivatives of the unknown disturbances have upper bounds:

$$\left\|\ddot{\zeta}\right\| \leq \delta \tag{24}$$

We have:

$$\dot{V} \leq -(2k + k)\vartheta^T\vartheta - \frac{1}{k}\delta^2 \tag{25}$$

To ensure that the system is asymptotically stable, we need:

$$\begin{aligned} \dot{V}(\vartheta) &= -3\kappa\vartheta^T\vartheta - \frac{1}{\kappa}\delta^2 \leq 0 \\ 3\kappa\|\vartheta\|^2 &\geq \frac{1}{\kappa}\delta^2 \\ \|\vartheta\|^2 &\leq \frac{\delta^2}{3\kappa^2} \end{aligned} \tag{26}$$

Since $\frac{1}{\kappa}\delta^2$ is constant, we have:

$$\begin{aligned} V(t) &\leq V(0)e^{-3\kappa t} \\ &= \zeta(0)e^{-3\kappa t} \end{aligned} \tag{27}$$

Therefore, if $\kappa > 0$, ϑ exponentially converges to 0. Based on Lemma 1, a disturbance observer can be designed to observe the acceleration disturbances in the system. For the system (16), the disturbance observer can be expressed as:

$$\dot{\hat{\zeta}} = \kappa\Big(X - X_{Lf}\Big) - U_f \tag{28}$$

□

Remark 2. *In the design of the disturbance observer, the acceleration information of the track rotation is not directly used as input. Instead, a low-pass filter is applied to implicitly include the track rotational speed-related state vector in the observer. This approach fully utilizes the observable information of the system while avoiding the differentiation of the velocity signal, effectively reducing noise amplification.*

Using the estimates of ζ_v and ζ_ω, the expression for the slip ratio can be derived by solving Equations (13) and (14) simultaneously:

$$\begin{aligned} s_l &= 1 - \frac{2\overline{v}_L - b\overline{\omega}_L + 2\zeta_v - b\zeta_\omega}{2\omega_l r} \\ s_r &= 1 - \frac{2\overline{v}_L - b\overline{\omega}_L + 2\zeta_v - b\zeta_\omega}{2\omega_r r} \end{aligned} \tag{29}$$

3.2. Path Following Controller

Lemma 2. *For a nonlinear system, if there exists a $\mathbb{C}^+$ function $V(x) > 0$ such that*

$$\dot{V}(x) \leq -cV^\alpha(x) - bV(x), x \in D/\{0\} \tag{30}$$

where $c > 0$, $b > 0$, $0 < \alpha < 1$, then the system is finite-time stable.

Lemma 3. *Considering a nonlinear system, if there exists a $\mathbb{C}^+$ function $V(x) > 0$ satisfying:*

$$\dot{V}(x) \leq -cV^\alpha(x), x \in D/\{0\} \tag{31}$$

where $c > 0$, $0 < \alpha < 1$, then the system is finite-time stable.

Since the speed of the track can be directly obtained through the encoder, a hierarchical control strategy is adopted for path following control: the upper-level controller is responsible for the whole vehicle kinematics path following, with the track rotation speed as the virtual control quantity; the lower-level controller is responsible for the dynamic track speed control, with the motor drive torque as the control input.

Define position error and attitude error:

$$e_L = \begin{pmatrix} e_{xL} \\ e_{yL} \\ e_{\varphi L} \end{pmatrix} = \begin{pmatrix} \cos\varphi & \sin\varphi & 0 \\ -\sin\varphi & \cos\varphi & 0 \\ 0 & 0 & 1 \end{pmatrix} \begin{pmatrix} x - x_d \\ y - y_d \\ \varphi - \varphi_d \end{pmatrix} \tag{32}$$

Design an integral sliding surface:

$$s = \begin{pmatrix} s_1 \\ s_2 \\ s_3 \end{pmatrix} = \begin{pmatrix} e_{xL} + \lambda_1 \int e_{xL} dt \\ e_{yL} + \lambda_1 \int e_{yL} dt \\ e_{\varphi L} + \lambda_1 \int e_{\varphi L} dt \end{pmatrix} \tag{33}$$

where $\lambda_1 > 0$ is a constant used to adjust the weight of the sliding surface. Calculate the derivative of the sliding surface s:

$$\dot{s} = \begin{pmatrix} \dot{s}_1 \\ \dot{s}_2 \\ \dot{s}_3 \end{pmatrix} = \begin{pmatrix} \dot{e}_{xL} + \lambda_1 e_{xL} \\ \dot{e}_{yL} + \lambda_1 e_{yL} \\ \dot{e}_{\varphi L} + \lambda_1 e_{\varphi L} \end{pmatrix} \tag{34}$$

The error dynamics can be expressed as:

$$\begin{aligned} \dot{e}_{xL} &= -\lambda_1 e_{xL} = \tfrac{r}{2}((1 - s_l)\omega_l + (1 - s_r)\omega_r)\cos\varphi \\ \dot{e}_{yL} &= -\lambda_1 e_{yL} = \tfrac{r}{2}((1 - s_l)\omega_l + (1 - s_r)\omega_r)\sin\varphi \\ \dot{e}_{\varphi L} &= -\lambda_1 e_{\varphi L} = \tfrac{r}{b}((1 - s_l)\omega_l - (1 - s_r)\omega_r) \end{aligned} \tag{35}$$

The rotational speeds of the left and right wheels are equivalent control outputs and can be represented as:

$$\begin{aligned} \omega_{left}^{eq} &= \tfrac{2\lambda_1(e_{xL}\cos\varphi + e_{yL}\sin\varphi) + \lambda_1 e_{\varphi L} b}{2r(1 - s_l)} \\ \omega_{right}^{eq} &= \tfrac{2\lambda_1(e_{xL}\cos\varphi + e_{yL}\sin\varphi) - \lambda_1 e_{\varphi L} b}{2r(1 - s_r)} \end{aligned} \tag{36}$$

The switching control outputs for the left and right wheel speeds can be expressed as:

$$u_{sw} = \begin{pmatrix} u_{sw,x} \\ u_{sw,y} \\ u_{sw,\varphi} \end{pmatrix} = \begin{pmatrix} -k_1 |s_1|^{1/2} \sin(s_1) - k_2 s_1 + s_2 \\ -k_3 |s_2|^{1/2} \sin(s_2) - k_4 s_2 + s_3 \\ -k_5 |s_3|^{1/2} \sin(s_3) - k_6 s_3 + s_1 \end{pmatrix} \tag{37}$$

To make the gains k_1, k_2, k_3, k_4, k_5, k_6 adaptively adjust, we introduce adaptive laws:

$$\begin{aligned} \dot{k}_1 &= \alpha_1 |s_1|^{1/2}, \dot{k}_2 = \alpha_2 |s_1| \\ \dot{k}_3 &= \alpha_1 |s_2|^{1/2}, \dot{k}_4 = \alpha_2 |s_2| \\ \dot{k}_5 &= \alpha_1 |s_3|^{1/2}, \dot{k}_6 = \alpha_2 |s_3| \end{aligned} \tag{38}$$

where α_1, α_2 are positive adaptive gain constants. The virtual control outputs for the left and right wheel speeds are:

$$\begin{aligned} \omega_l^* &= \omega_l^{eq} + u_{sw,x} + u_{sw,y} + u_{sw,\varphi} \\ \omega_r^* &= \omega_r^{eq} + u_{sw,x} + u_{sw,y} - u_{sw,\varphi} \end{aligned} \tag{39}$$

Remark 3. *The specific approach to adaptive gain design involves introducing an adaptive law to dynamically adjust the control gain based on the system's real-time state and error information. This allows the gain to adaptively respond to uncertainties in system parameters, external disturbances, and nonlinear characteristics. The logic is grounded in Lyapunov stability theory: a Lyapunov*

function candidate is first defined, incorporating both the sliding mode variable and the gain error. An adaptive law, such as an update rule for the gain, is then designed such that the derivative of this function is non-positive, ensuring system stability. The role of the adaptive gain is to dynamically adjust the gain value, enabling the sliding mode variable to rapidly converge to zero (i.e., reach the switching surface) and remain stable on the surface, while avoiding excessive control inputs or chattering phenomena. Consequently, adaptive gain not only enhances the robustness of the controller but also optimizes the system's dynamic performance, ensuring stable and efficient control across various operating conditions.

Proof. Consider the Lyapunov function V_{s1}:

$$V_{s1} = \frac{1}{2}(s^T s + s^T \dot{s}) \tag{40}$$

Taking the derivative:

$$\dot{V}_{s1} = s^T \dot{s} + \dot{s}^T \ddot{s} \tag{41}$$

Substituting the controller design (37):

$$\dot{V}_{s1} = s^T(-K_1|s|_{1/2}\sin(s) - K_2 s + s) + \dot{s}^T\left(-K_3\left|s\right|_{1/2} - K_4 s + \ddot{s}\right) \tag{42}$$

where:

$$\begin{array}{rl} K_1 & = \begin{pmatrix} k_1 & 0 & 0 \\ 0 & k_3 & 0 \\ 0 & 0 & k_5 \end{pmatrix}, K_2 = \begin{pmatrix} k_2 & 0 & 0 \\ 0 & k_4 & 0 \\ 0 & 0 & k_6 \end{pmatrix} \\ K_3 & = \begin{pmatrix} 0 & 0 & 0 \\ 0 & 0 & 0 \\ 0 & 0 & \lambda_1 \end{pmatrix}, K_4 = \begin{pmatrix} 0 & 0 & 0 \\ 0 & 0 & 0 \\ 0 & 0 & \lambda_2 \end{pmatrix} \end{array} \tag{43}$$

Further expansion:

$$\dot{V}_{s1} = -s^T K_1\left|s\right|_{1/2}\sin(s) - s^T K_2 s + s^T\dot{s} - \dot{s}^T K_3\left|s\right|_{1/2} - \dot{s}^T K_4 s + \dot{s}^T\ddot{s} \tag{44}$$

Substituting the adaptive gain laws (38):

$$\begin{array}{l} \dot{V}_{s1} = s^T\left(-K_1\left|s\right|_{1/2}\sin(s) - K_2 s + \dot{s}\right) + \dot{s}^T\left(-K_3\left|s\right|_{1/2} - K_4 s + \ddot{s}\right) \\ -s^T\left(\frac{\partial u}{\partial k}\right)^T\begin{pmatrix} \dot{k}_1 & \dot{k}_2 & \dot{k}_3 & \dot{k}_4 & \dot{k}_5 & \dot{k}_6 \end{pmatrix}^T \end{array} \tag{45}$$

where:

$$\frac{\partial u}{\partial k} = \begin{pmatrix} -|s_1|^{1/2}\sin(s_1) & -s_1 & 0 & 0 & 0 & 0 \\ 0 & 0 & -|s_2|^{1/2}\sin(s_2) & -s_2 & 0 & 0 \\ 0 & 0 & 0 & 0 & -|s_3|^{1/2}\sin(s_3) & -s_3 \end{pmatrix} \tag{46}$$

Substituting into (45):

$$\begin{array}{rl} \dot{V}_{s1} & = s^T\left(-K_1\left|s\right|_{1/2}\sin(s) - K_2 s + \dot{s}\right) + \dot{s}^T\left(-K_3\left|s\right|_{1/2} - K_4 s + \ddot{s}\right) \\ & -2c_1\begin{pmatrix} s_1\left(-\frac{1}{2}|s_1|^{-1/2}s_1\sin(s_1) - |s_1|^{1/2}\cos(s_1)\right)|s_1|^{1/2} + \\ s_2\left(-\frac{1}{2}|s_2|^{-1/2}s_2\sin(s_2) - |s_2|^{1/2}\cos(s_2)\right)|s_2|^{1/2} + \\ s_3\left(-\frac{1}{2}|s_3|^{-1/2}s_3\sin(s_3) - |s_3|^{1/2}\cos(s_3)\right)|s_3|^{1/2} \end{pmatrix} \\ & -2c_2(s_1(-s_1)|s_1| - s_2(-s_2)|s_2| + s_3(-s_3)|s_3|) \\ & = s^T\left(-K_1\left|s\right|_{1/2}\sin(s) - K_2 s + \dot{s}\right) + \dot{s}^T\left(-K_3\left|s\right|_{1/2} - K_4 s + \ddot{s}\right) \\ & +2c_1\left(s_1^2|\sin(s_1)| + s_2^2|\sin(s_2)| + s_3^2|\sin(s_3)|\right) + 2c_2\left(s_1^2|s_1| + s_2^2|s_2| + s_3^2|s_3|\right) \end{array} \tag{47}$$

Substituting the adaptive gain laws (38):

$$\begin{aligned}\dot{V}_{s1} &= s^T\left(-K_1|s|^{1/2}\sin(s) - K_2 s + \dot{s}\right) + \dot{s}^T\left(-K_3|s|_{1/2} - K_4 s + \ddot{s}\right)\\ &-s^T\left(\frac{\partial u}{\partial k}\right)^T\begin{pmatrix}\alpha_1|s_1|^{1/2} & \alpha_2|s_1| & \alpha_3|s_2|^{1/2} & \alpha_4|s_2| & \alpha_5|s_3|^{1/2} & \alpha_6|s_3|\end{pmatrix}^T\end{aligned} \tag{48}$$

Choose $\alpha_1 = 2c_1$, $\alpha_2 = 2c_2$, where c_1, c_2 are positive constants. Substituting, we get:

$$\begin{aligned}&\dot{V}_{s1} = s^T\left(-K_1|s|^{1/2}\sin(s) - K_2 s + \dot{s}\right) + \dot{s}^T\left(-K_3|s|^{1/2} - K_4 s + \ddot{s}\right)\\ &-s^T\left(\frac{\partial u}{\partial k}\right)^T\begin{pmatrix}2c_1|s_1|^{1/2} & 2c_2|s_1| & 2c_1|s_2|^{1/2} & 2c_2|s_2| & 2c_1|s_3|^{1/2} & 2c_2|s_3|\end{pmatrix}^T\\ &= s^T\left(-K_1|s|^{1/2}\sin(s) - K_2 s + s\right) + s^T\left(-K_3|s|^{1/2} - K_4 s + s\right)\\ &-2c_1 s^T\left(\frac{\partial u}{\partial k}\right)^T\begin{pmatrix}|s_1|^{1/2} & 0 & |s_2|^{1/2} & 0 & |s_3|^{1/2} & 0\end{pmatrix}^T\\ &-2c_2 s^T\left(\frac{\partial u}{\partial k}\right)^T\begin{pmatrix}0 & |s_1| & 0 & |s_2| & 0 & |s_3|\end{pmatrix}^T\end{aligned} \tag{49}$$

Substitute (46) into it:

$$\begin{aligned}\dot{V}_{s1} &= s^T\left(-K_1|s|^{1/2}\sin(s) - K_2 s + \dot{s}\right) + +\dot{s}^T(-K_3|s|^{1/2} - K_4 s + \ddot{s})\\ &+2c_1\left(s_1^2|\sin(s_1)| + s_2^2|\sin(s_2)| + s_3^2|\sin(s_3)|\right)\\ &+2c_2\left(s_1^2|s_1| + s_2^2|s_2| + s_3^2|s_3|\right)\end{aligned} \tag{50}$$

To ensure that $\dot{V}_{s1}$ is negative definite, choose appropriate c_1, c_2 such that:

$$\dot{V}_{s1} \le -c_1 V_{s1}^{1/2} - c_2 V_{s1} \tag{51}$$

At this time,

$$\alpha_1 = 2c_1, \alpha_2 = 2c_2 \tag{52}$$

where the gains k_1, k_2, k_3, k_4, k_5, k_6 are updated through adaptive laws. □

3.3. Wheel Speed Controller

The lower-level controller is responsible for dynamic track speed control, with the motor drive torque as the control input. Define the speed error:

$$\begin{aligned}e_{\omega,l} &= \omega_l - \omega_l^*\\ e_{\omega,r} &= \omega_r - \omega_r^*\end{aligned} \tag{53}$$

where ω_l^* and ω_r^* are the desired speeds of the left and right tracks. Assume that the speeds of each track, ω_l and ω_r, are controlled by the motor drive torques T_l and T_r, respectively. Use the dynamic model (13). Define the angular acceleration error:

$$\begin{aligned}\dot{e}_{\omega,l} &= \dot{\omega}_l - \dot{\omega}_l^*\\ \dot{e}_{\omega,r} &= \dot{\omega}_r - \dot{\omega}_r^*\end{aligned} \tag{54}$$

Define the super-twisting sliding mode as [27]:

$$\begin{aligned}\dot{s}_{s,l} &= -\mu_1|x_1|_{1/2}\sin(x_1) + \mu_2 x_2 + \rho_1(x,t)\\ \ddot{s}_{s,l} &= -\mu_3\sin(x_1) + \rho_2(x,t)\\ \dot{s}_{s,r} &= -\mu_1|x_1|_{1/2}\sin(x_1) + \mu_2 x_2 + \rho_1(x,t)\\ \ddot{s}_{s,r} &= -\mu_3\sin(x_1) + \rho_2(x,t)\end{aligned} \tag{55}$$

where ρ_1 and ρ_2 are unknown disturbances. The control input can be expressed as:

$$\begin{aligned} T_{e,l} &= J\left(\omega_l^* + (-\mu_1|x_1|_{1/2}\sin(x_1) + \mu_2 x_2) + \mu_\omega \omega_l\right) + \mu_3 J_l \sin(x_1) + \mu_4 sat\left(\frac{x_1}{\delta_s}\right) \\ T_{e,r} &= J(\omega_r^* + (-\mu_1|x_1|_{1/2}\sin(x_1) + \mu_2 x_2) + \mu_\omega \omega_r) + \mu_3 J_r \sin(x_1) + \mu_4 sat\left(\frac{x_1}{\delta_s}\right) \end{aligned} \tag{56}$$

where:

$$sat\left(\frac{x_1}{\delta}\right) = \begin{cases} \frac{x_1}{\delta} & \text{if} |x_1| \le \delta_s \\ sign(x_1) & \text{if} |x_1| > \delta_s \end{cases} \tag{57}$$

Proof. We choose the Lyapunov function V_{s2} as

$$V_{s2} = \frac{1}{2}\mu_2 x_2^2 + \frac{2}{3}\mu_1 |x_1|^{3/2} \tag{58}$$

Compute the derivative of the Lyapunov function V_{s2}, denoted as $\dot{V}_{s2}$:

$$\dot{V}_{s2} = \mu_2 x_2 \dot{x}_2 + \mu_1 |x_1|^{1/2} sign(x_1)\dot{x}_1 \tag{59}$$

Substitute $\dot{x}_1$ and $\dot{x}_2$:

$$\begin{aligned} \dot{V}_{s3} &= \mu_2 x_2(-\mu_3 \sin(x_1) + \rho_2(x,t)) + \mu_1 |x_1|^{1/2} sign(x_1)(-\mu_1 |x_1|^{1/2}\sin(x_1) + x_2 + \rho_1(x,t)) \\ &= -\mu_2\mu_3 x_2 \sin(x_1) + \mu_2 x_2 \rho_2(x,t) - \mu_2 \mu_1^2 |x_1| \sin(x_1) + \mu_1 \mu_2 x_2 |x_1|^{1/2} \\ &+ \mu_1 \mu_2 |x_1|^{1/2} sign(x_1)\rho_1(x,t) \end{aligned} \tag{60}$$

Consider the boundedness of ρ_1 and ρ_2, which represent the difference between the driving force and resistance of a single track, and both the difference and its derivative are bounded. Assume:

$$|\rho_1(x,t)| \le \Delta_1, |\rho_2(x,t)| \le \left|\dot{\Delta}_1\right| \tag{61}$$

where Δ_1 is a known positive bound. Substitute these bounds into $\dot{V}_{s3}$:

$$\dot{V}_{s3} \le -\mu_3 x_2 \sin(x_1) + \mu_2 x_2 \dot{\Delta}_1 - \mu_1^2 |x_1| \sin(x_1) + \mu_1 x_2 |x_1|^{1/2} + \mu_1 \Delta_1 |x_1|^{1/2} \tag{62}$$

To ensure that $\dot{V}_{s3}$ is negative definite, choose:

$$\begin{aligned} \mu_2\mu_3 &> \dot{\Delta}_1 \\ \mu_1 &> \Delta_1 \end{aligned} \tag{63}$$

Such that V_{s2} remains stable on the sliding mode. The specific form can be expressed as:

$$\dot{V} \le -\eta V \tag{64}$$

where η is a positive constant. According to Lemma 3, this implies that the system approaches the sliding mode in finite time, and by the Lyapunov stability theorem, if $\dot{V}_{s3}$ is negative definite, the system is asymptotically stable. Therefore, the designed super-twisting sliding mode control law ensures the robustness and stability of the track robot's speed control system. □

Through this design, the speed tracking controller of the tracked vehicle can handle dynamic issues and ensure that the position and attitude errors converge to zero in finite time. This hierarchical control strategy enhances the system's robustness and tracking accuracy.

4. Validation of Effectiveness

To validate the effectiveness of the proposed TMR trajectory tracking control scheme, control performance testing was conducted through both simulation and experimental methods.

4.1. Simulation

In the Simulink simulation environment, MATLAB 2022b was used to construct the dynamic model of the TMR, including its kinematic model and the dynamic model of the tracks. Through Simulink's modular design, it is convenient to implement trajectory tracking control strategies such as PID control and SMC control. During the simulation, an internal signal generator module was utilized to generate various test signals, and the real-time data monitoring and post-processing were performed using the data acquisition and analysis toolbox, ensuring the performance of the control algorithm was effectively validated. Table 1 presents the key parameters of the TMR. Table 2 presents the key parameters of the controllers.

Table 1. Key parameters of the model.

Parameter	Value
Total Mass M	16.3 kg
Track Spacing	65 cm
Track Width	11 cm
Track Contact Length	68.1 cm
Drive Wheel Radius	10 cm

Table 2. Key parameters of the controller.

Parameter	Value	Parameter	Value
Observer Gain κ	100	Speed Controller Gain μ_2	2
Adaptation Gain α_1	10	Speed Controller Gain μ_3	7
Adaptation Gain α_2	5	Disturbance Term Gain μ_4	25
Sliding Surface Gain λ_1	3	PID Controller k_p	15
Speed Controller Gain μ_1	1.5	PID Controller k_i	1

Using a PID controller as the control group, Figures 4–6 show the motion trajectory curves of the TMR under the influence of both controllers. The desired trajectory is given by:

$$\begin{cases} x_d(t) = 5 \cdot \cos(0.2t + \frac{\pi}{2}) \\ y_d(t) = 3 \cdot \cos(0.4t + \frac{\pi}{2}) \\ \varphi_d(t) = \arctan2(-2 \cdot 3 \cdot 0.2 \cdot \sin(0.4t + \frac{\pi}{2}), -5 \cdot 0.2 \cdot \sin(0.2t + \frac{\pi}{2})) \end{cases} \tag{65}$$

Figure 4a illustrates that both controllers can effectively track the desired trajectory in the simulation environment, with a slight initial deviation in the trajectory of the PID controller. The experiment tracking path is shown in Figure 4b, with the desired path consistent with Equation (65). Under the proposed SMC control, the TMR can follow the desired trajectory.

Figure 5 shows that both controllers exhibit a certain degree of deviation at the initial stage, which is due to an initial pose offset of 0.1 m set to test the influence of initial conditions on controller performance. In Figure 5a, both controllers can follow the desired trajectory, while Figure 5b provides a magnified view of the turning trajectory, indicating that the proposed SMC-based tracking trajectory has a smaller turning deviation compared to the PID controller. Figure 5c is a magnified view of the initial stage trajectory, showing that the SMC controller converges faster than the PID controller and effectively follows the

desired trajectory after a single oscillation. Figure 5d displays the tracking error distribution curves of both controllers, where the SMC curve, although showing some fluctuations, has a smaller error range and peak error compared to the PID controller, demonstrating its performance advantage.

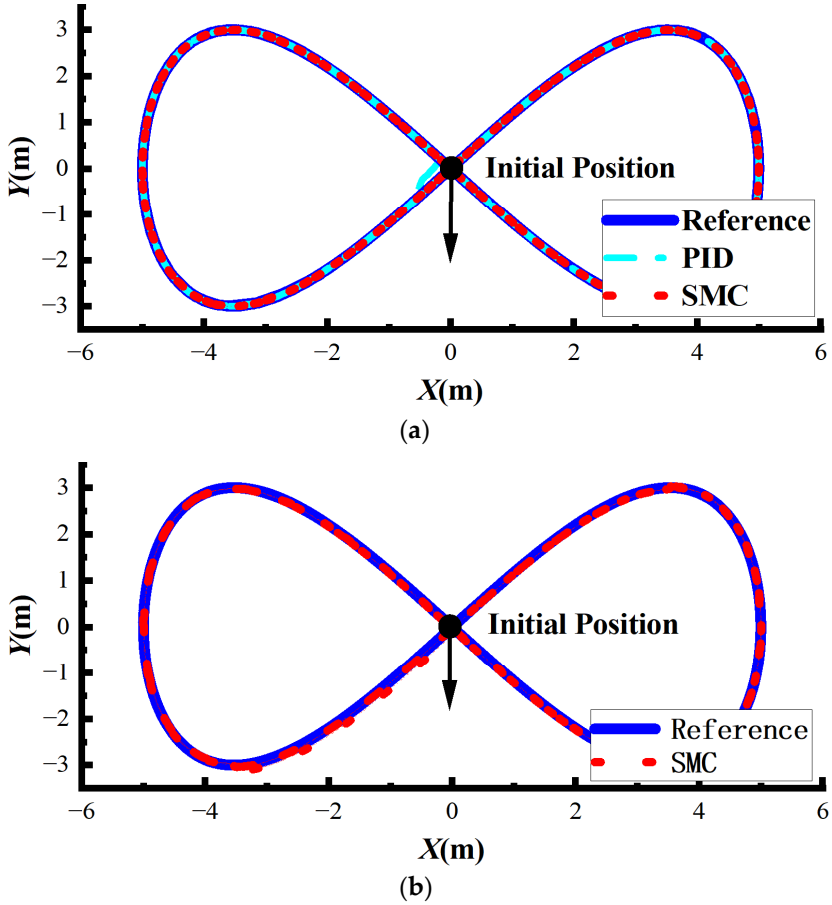

Figure 4. Simulation and Experiment Tracking Trajectory of "8" Path. (**a**) Simulation result, (**b**) Experiment result.

Figure 6 presents the tracking curves of both controllers in the *X*-direction. Among them, Figure 6a is the tracking path curve; Figure 6b is the magnified view of the turning path; Figure 6c is the magnified view of the initial stage; and Figure 6d is the tracking error distribution curve. The tracking performance of both controllers in the *X*-direction is consistent with that in the *Y*-direction and is not discussed further here.

Figure 7 illustrates the observed values of the left sliding coefficient. To test the performance of the observer, the left sliding coefficient was set as $S_{l,r} = 0.2 \cos(t)$, and the observed values steadily follow the provided reference values. Figure 7b shows the distribution of the observation error. Except at the beginning of the motion, the maximum error does not exceed 0.07, indicating that the observer can accurately estimate the sliding coefficient and compensate for the controller. The research method for the right sliding coefficient is the same as for the left and is not discussed further here.

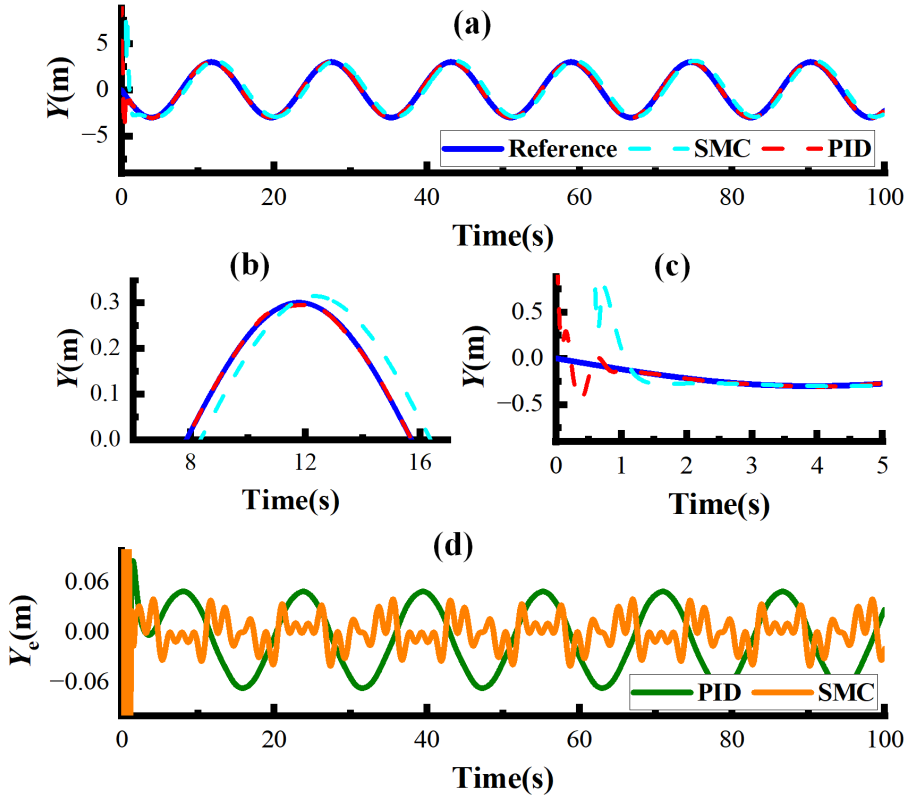

Figure 5. *Y*-Direction Trajectory Tracking Performance Curves.

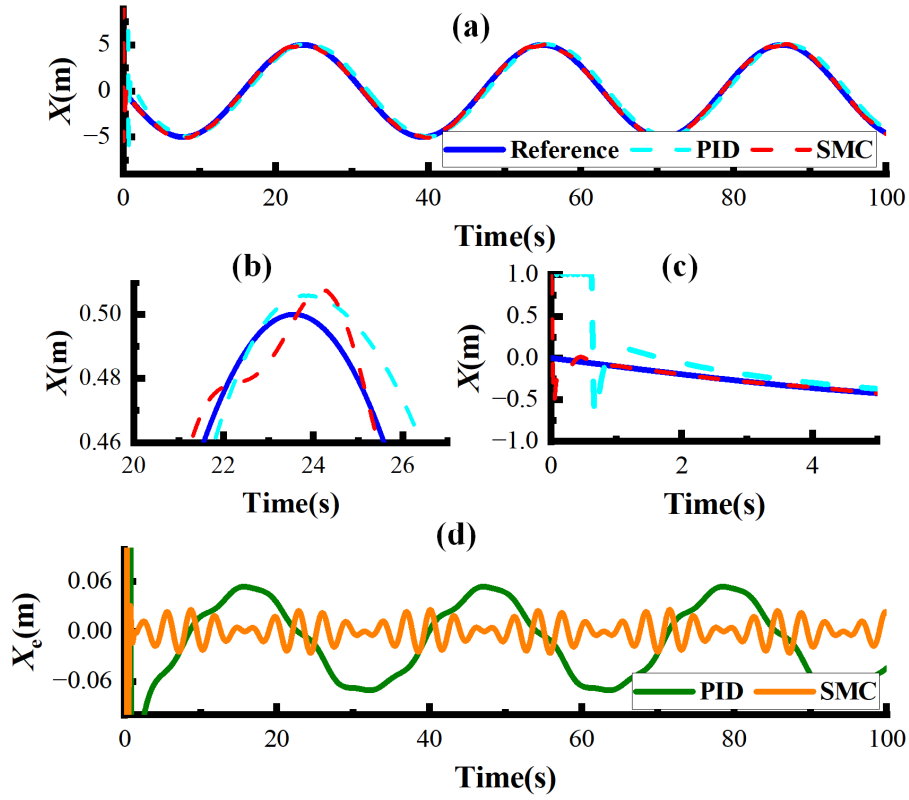

Figure 6. *X*-Direction Trajectory Tracking Performance Curves.

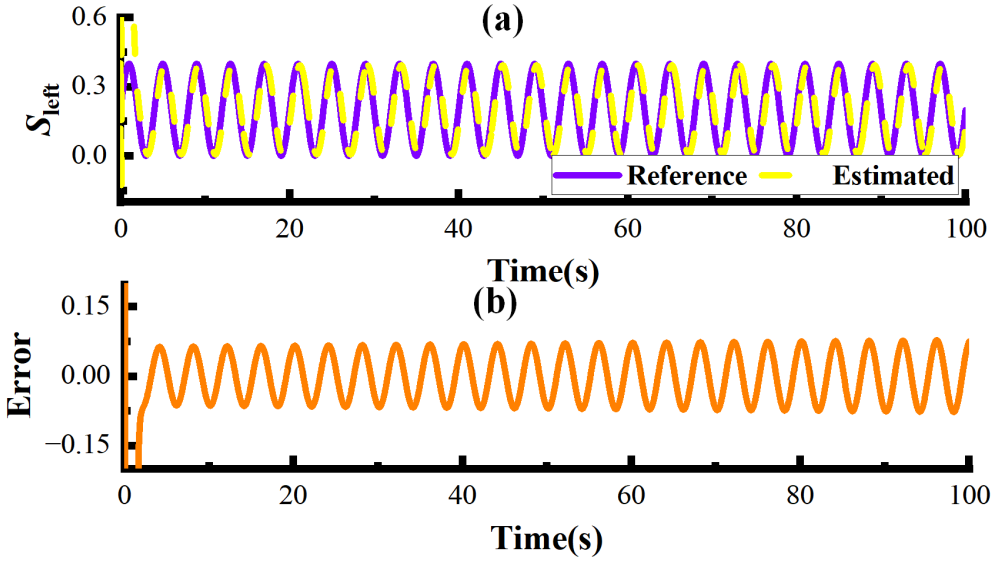

Figure 7. Disturbance Observer Estimation Curves. (**a**) The input and observed value change curve for the left sliding factor, (**b**) the observed error of the sliding factor.

As shown in Table 3, in trajectory tracking control, both the Sliding Mode Control (SMC) controller and the Proportional-Integral-Derivative (PID) controller have their advantages and disadvantages. The SMC controller offers high precision, robustness, and good dynamic performance, making it suitable for complex environments. However, it has longer computation times and higher hardware and development costs. The PID controller, on the other hand, has shorter computation times and lower hardware and development costs, making it suitable for simple environments. However, it has larger trajectory tracking errors and poorer dynamic performance, often leading to oscillations or instability in complex environments.

Table 3. Detailed Comparison of SMC and PID.

Performance Metrics	SMC Controller	PID Controller
Computation Time	17.5 s	11 s
Maximum Error	0.2 m	0.5 m
Average Error	0.05 m	0.12 m
Mean Squared Error	0.005 square meters	0.03 square meters
Suitable Environment	Complex environments (nonlinear, external disturbances)	Simple environments (linear, low disturbances)

4.2. Experiment

To validate the effectiveness of the TMR trajectory tracking control scheme, the experimental environment employs the Ublox ZED-F9P-01B high-precision GPS receiver, providing centimeter-level positioning accuracy to ensure the robot's position information is accurate. Additionally, a Heidenhain ECN 413 2048 16S15-2K incremental encoder with an accuracy of 0.001 degrees/pulse is used to monitor the rotation of the tracks in real-time, ensuring precise speed and position control. The main controller uses a Siemens S7-1200 PLC, supporting fast data acquisition and processing with a response time of less than 1 ms. The wireless communication terminal is the DTD418MA, and data acquisition and processing are achieved through the NI USB-6363 data acquisition card, which supports multi-channel synchronous sampling with adjustable sampling rates, ensuring the integrity and precision of the data. Figure 8 shows the TMR experimental platform,

where the experimental site is a lawn, fully testing the control performance under track sliding conditions.

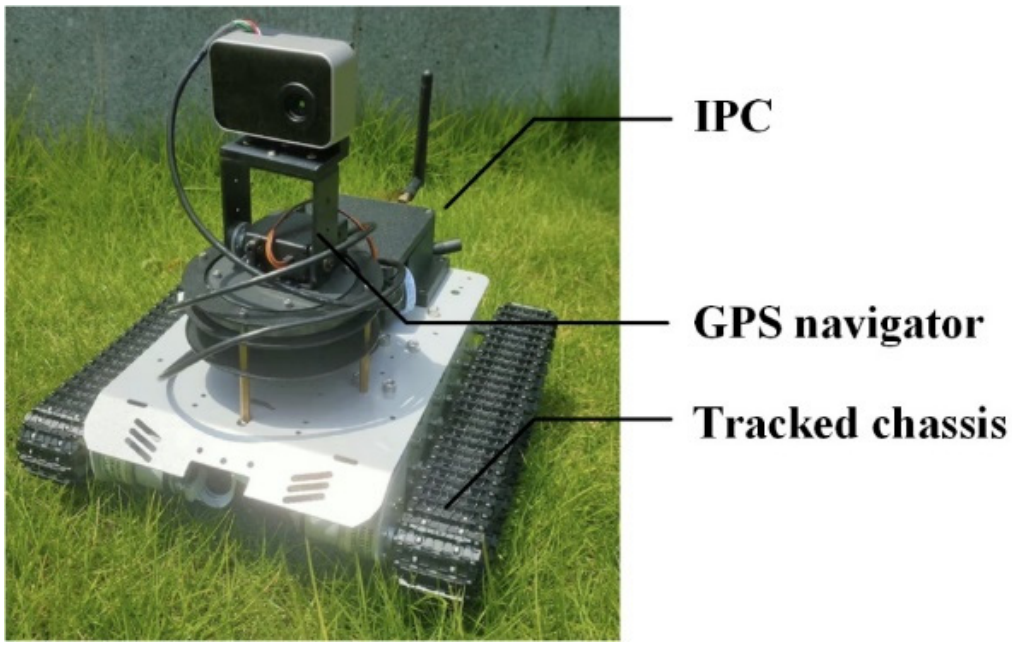

Figure 8. TMR Experimental Platform.

Figure 9 illustrates that Figure 9a,c respectively, show the distribution curves of the tracking trajectory in the X and Y directions; Figure 9b,d respectively, show the error distribution curves of the tracking trajectory in the X and Y directions. It can be seen that except for the initial motion phase, the maximum error does not exceed 0.08 m, with a slight increase in error compared to the simulation results, likely due to sensor errors and signal noise. Figure 9e shows the observed value of the left sliding factor, indicating that the sliding is initially severe, but gradually stabilizes around 0.1 as the tracking progresses. Figure 9f shows the speed distribution curves of the left and right wheels, indicating that under the SMC control, the speeds of both driving wheels are within the range of 5–20 rad/s, with smooth speed curves that do not exceed the actuator's performance capabilities.

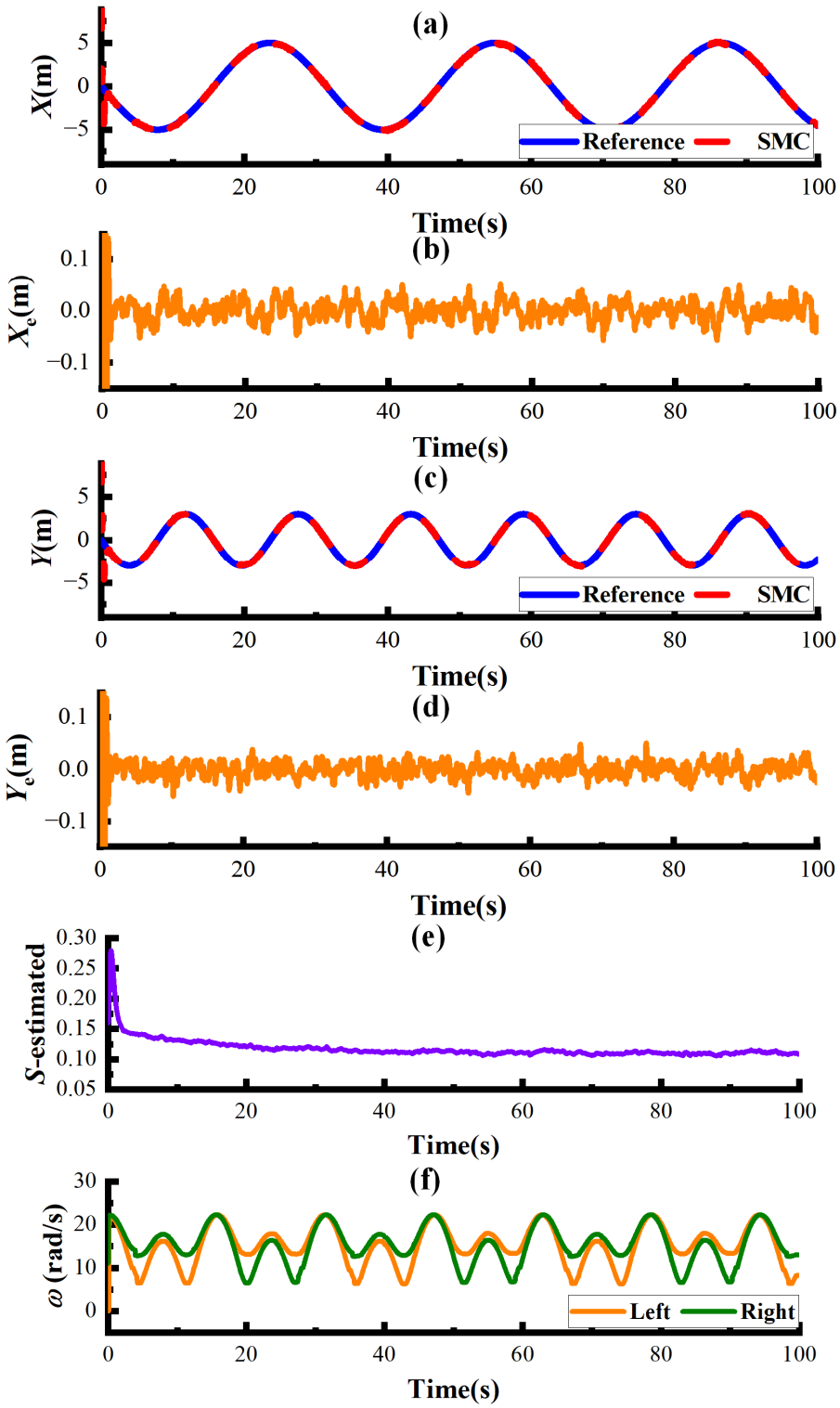

Figure 9. Experimental Result Curves. (**a**) The change curve of the displacement component in the *X* direction, (**b**) the error component in the *X* direction, (**c**) the change curve of the displacement component in the *Y* direction, (**d**) the error component in the *Y* direction, (**e**) the estimated value of the sliding factor on the left side, (**f**) the speed change curve of the left and right driving wheels.

5. Conclusions

This paper proposes a hierarchical trajectory tracking control scheme for track robots, providing a kinematic and dynamic model of the TMR considering sliding. The sliding factor is treated as an external disturbance, and a disturbance observer is designed and

proven to be stable, with only one adjustable parameter, facilitating practical application. A super-twisting sliding mode controller is designed to separately control the speed and torque of the left and right driving wheels, effectively avoiding sliding mode chattering. Both simulation and experimental validation demonstrate the performance of the proposed controller, showing that the SMC's convergence time, mean error, and peak error are all smaller than the control group, compared to PID, proposed SMC increases computation time by 40%, but the tracking accuracy improves by 200%, exhibiting beneficial control performance.

Since this study was conducted on a flat, unpaved surface, future research should further consider the impact of ground unevenness to enhance the TMRs' adaptability to working environments.

Author Contributions: Conceptualization, X.Y.; Methodology, S.W.; Software, S.W. and A.M.; Validation, Y.H. and A.M.; Writing—original draft, X.Y.; Writing—review & editing, Y.H.; Supervision, S.Z. All authors have read and agreed to the published version of the manuscript.

Funding: The authors have not disclosed any funding.

Data Availability Statement: All data generated or analyzed during this study are included in this published article.

Conflicts of Interest: The author declares no conflicts of interest.

References

1. Wang, P.; Rui, X.; Gu, J.; Huang, K.; Zhou, L.; Jiang, M. Fast parametric modeling of visualized simulation and design for tracked vehicle system. *Adv. Eng. Softw.* **2025**, *201*, 103852. [CrossRef]
2. Shentu, S.; Xie, F.; Liu, X.J.; Gong, Z. Motion Control and Trajectory Planning for Obstacle Avoidance of the Mobile Parallel Robot Driven by Three Tracked Vehicles. *Robotica* **2020**, *39*, 1037–1050. [CrossRef]
3. Subari, M.A.; Hudha, K.; Kadir, Z.A.; Dardin, S.M.F.B.S.M.; Amer, N.H. Development of path tracking control of a tracked vehicle for an unmanned ground vehicle. *Int. J. Adv. Mechatron. Syst.* **2021**, *8*, 136–143. [CrossRef]
4. Chen, Y.; Zhang, H.; Zou, W.; Zhang, H.; Zhou, B.; Xu, D. Dynamic modeling and learning based path tracking control for ROV-based deep-sea mining vehicle. *Expert Syst. Appl.* **2025**, *262*, 125612. [CrossRef]
5. Ahmad, A.J.; Mohammad, S. Trajectory tracking control of tracked vehicles considering nonlinearities due to slipping while skid-steering. *Syst. Sci. Control Eng.* **2022**, *10*, 887–898.
6. Wong, J.Y. Dynamics of tracked vehicles. *Veh. Syst. Dyn.* **1997**, *28*, 197–219. [CrossRef]
7. Dimauro, L.; Venturini, S.; Tota, A.; Galvagno, E.; Velardocchia, M. High-speed tracked vehicle model order reduction for static and dynamic simulations. *Def. Technol.* **2024**, *38*, 89–110. [CrossRef]
8. Ilango, M.; Chandramouli, P. An integrated three-dimensional powertrain-vehicle dynamics model for tracked vehicle analysis. *Proc. Inst. Mech. Eng. Part D J. Automob. Eng.* **2023**, *237*, 3353–3366.
9. Zhiqiang, G.; Sihai, Z.; Junlin, L. Modelling and analysis of longitudinal-vertical coupling dynamics for the tracked vehicle on uneven roads. *Proc. Inst. Mech. Eng. Part D J. Automob. Eng.* **2023**, *237*, 2885–2898.
10. Hou, X.; Ma, Y.; Xiang, C. Design and comparative study of steering controller for tracked vehicle based on disturbance observation. *Proc. Inst. Mech. Eng. Part D J. Automob. Eng.* **2024**, *238*, 4216–4229. [CrossRef]
11. Chen, Z.; Hu, S.; Lv, H.; Fu, Y. A Novel Estimating Algorithm of Critical Driving Parameters for Dual-Motor Electric Drive Tracked Vehicles Based on a Nonlinear Observer and an Adaptive Kalman Filter. *Energies* **2024**, *17*, 4625. [CrossRef]
12. Zhao, X.; Lu, E.; Tang, Z.; Luo, C.; Xu, L.; Wang, H. Trajectory prediction method for agricultural tracked robots based on slip parameter estimation. *Comput. Electron. Agric.* **2024**, *222*, 109057. [CrossRef]
13. Letizia, C.M. Data Driven Control and slip estimation for Agricultural Tracked Vehicles. *Franklin Open* **2023**, *5*, 100048.
14. Hu, K.; Cheng, K. Trajectory Planning for an Articulated Tracked Vehicle and Tracking the Trajectory via an Adaptive Model Predictive Control. *Electronics* **2023**, *12*, 1988. [CrossRef]
15. Sabiha, A.D.; Kamel, M.A.; Said, E.; Hussein, W.M. Dynamic modeling and optimized trajectory tracking control of an autonomous tracked vehicle via backstepping and sliding mode control. *Proc. Inst. Mech. Eng. Part I J. Syst. Control. Eng.* **2022**, *236*, 620–633. [CrossRef]
16. Cao, Y.; Pu, J. A Novel Zeroing Neural Network Control Scheme for Tracked Mobile Robot Based on an Extended State Observer. *Appl. Sci.* **2023**, *14*, 303. [CrossRef]

17. Xu, Q. Digital integral terminal sliding mode predictive control of piezoelectric-driven motion system. *IEEE Trans. Ind. Electron.* **2015**, *63*, 3976–3984. [CrossRef]
18. Jin, M.; Lee, J.; Chang, P.H.; Choi, C. Practical nonsingular terminal sliding-mode control of robot manipulators for high-accuracy tracking control. *IEEE Trans. Ind. Electron.* **2009**, *56*, 3593–3601.
19. Chalanga, A.; Kamal, S.; Fridman, L.M.; Bandyopadhyay, B.; Moreno, J.A. Implementation of Super-Twisting Control: Super-Twisting and Higher Order Sliding-Mode Observer-Based Approaches. *IEEE Trans. Ind. Electron.* **2016**, *63*, 3677–3685. [CrossRef]
20. Huiming, W.; Yang, Z.; Xuechuang, W.; Yue, F. Cascaded continuous sliding mode control for tracked mobile robot via nonlinear disturbance observer. *Comput. Electr. Eng.* **2022**, *97*, 107579.
21. Zeng, R.; Kang, Y.; Yang, J.; Wang, Z.; Li, G.; Cao, D. Learning-based terrain identification with proprioceptive sensors for mobile robots. *IEEE Trans. Ind. Electron.* **2020**, *68*, 8433–8443. [CrossRef]
22. Qin, Z.; Chen, L.; Fan, J.; Xu, B.; Hu, M.; Chen, X. An improved real-time slip model identification method for autonomous tracked vehicles using forward trajectory prediction compensation. *IEEE Trans. Instrum. Meas.* **2021**, *70*, 1–12. [CrossRef]
23. Subari, M.A.; Hudha, K.; Kadir, Z.A.; Dardin, S.M.F.S.M.; Amer, N.H. Path following control of tracked vehicle using modified sup controller optimized with particle swarm optimization (PSO). *Int. J. Dyn. Control.* **2022**, *10*, 1461–1470. [CrossRef]
24. Martínez, J.L.; Morales, J.; Mandow, A.; Pedraza, S.; García-Cerezo, A. Inertia-based ICR kinematic model for tracked skid-steer robots. In Proceedings of the 2017 IEEE International Symposium on Safety, Security and Rescue Robotics (SSRR), Shanghai, China, 11–13 October 2017; IEEE: New York, NY, USA, 2017; pp. 166–171.
25. Sabiha, A.D.; Kamel, M.A.; Said, E.; Hussein, W.M. ROS-based trajectory tracking control for autonomous tracked vehicle using optimized backstepping and sliding mode control. *Robot. Auton. Syst.* **2022**, *152*, 104058. [CrossRef]
26. Na, J.; Li, Y.; Huang, Y.; Gao, G.; Chen, Q. Output Feedback Control of Uncertain Hydraulic Servo Systems. *IEEE Trans Ind. Electron.* **2020**, *67*, 490–500. [CrossRef]
27. Moreno, J.A.; Osorio, M. A Lyapunov approach to second-order sliding mode controllers and observers. In Proceedings of the 2008 47th IEEE Conference on Decision and Control, Cancun, Mexico, 9–11 December 2008; IEEE: New York, NY, USA, 2008; pp. 2856–2861.